Research Square

Preprints are preliminary reports that have not undergone peer review.
They should not be considered conclusive, used to inform clinical practice,
or referenced by the media as validated information.

Establishment and Characterization of OK-ATC1 and OK-ATC1-PDX: a Novel Cell Line and Patient-Derived Xenograft Model of BRAF V600E-Mutated Anaplastic Thyroid Carcinoma

Yu Shimoda
Kumamoto Daigaku Byoin
Seiji Okada
Kumamoto Daigaku
Yukio Fujiwara
Kumamoto Daigaku Daigakuin Seimei Kagaku Kenkyuka Igakubu: Kumamoto Daigaku Daigakuin Seimei Kagaku Kenkyubu Igakubu
Winidmanokul Peeranut
Kumamoto Daigaku
Hiromi Ogata-Aoki
Kumamoto Daigaku
Kaori Yukino
Kumamoto Daigaku Byoin
Akira Murakami
Kumamoto Daigaku Byoin
Haruki Saito
Kumamoto Daigaku Byoin
Yoshihiro Komohara
Kumamoto Daigaku Daigakuin Seimei Kagaku Kenkyuka Igakubu: Kumamoto Daigaku Daigakuin Seimei Kagaku Kenkyubu Igakubu
Yorihisa Orita
y.orita@live.jp

Kumamoto Daigaku Daigakuin Seimei Kagaku Kenkyuka Igakubu: Kumamoto Daigaku Daigakuin Seimei Kagaku Kenkyubu Igakubu https://orcid.org/0000-0002-2803-9623

Research Article

Keywords: Anaplastic thyroid carcinoma (ATC), Patient-Derived Xenograft (PDX), BRAF V600E, TERT promoter − 146C > T, TP53 V73fs*50

Posted Date: November 6th, 2026

DOI: https://doi.org/10.21203/rs.3.rs-11448123/v1

License: This work is licensed under a Creative Commons Attribution 4.0 International License.
Read Full License

Abstract

Anaplastic thyroid carcinoma (ATC) is characterized by rapid progression, marked biological heterogeneity, and rarity, which makes clinical studies difficult to conduct. The development of novel therapeutic strategies for ATC thus requires appropriate experimental animal models. We established a novel ATC cell line (OK-ATC1) and corresponding patient-derived xenograft (PDX) model (OK-ATC1-PDX) from an 89-year-old Japanese female patient. The patient's ATC was diagnosed as having arisen from transformation of papillary thyroid carcinoma. Both the newly established cell line and PDX model successfully retained the immunohistochemical and genetic profiles of the clinical ATC component. Immunophenotypically, the models were p53-negative, PAX8-positive, and TTF-1–negative. Genetic profiling revealed that both OK-ATC1 and OK-ATC1-PDX maintained key driver mutations identified in the primary tumor, including *BRAF* V600E, *TERT* promoter − 146C > T, and *TP53* V73fs*50. To our knowledge, this is the first reported ATC-PDX model harboring a *TERT* promoter − 146C > T mutation, and this is one of the few studies to have simultaneously established both an ATC cell line and PDX model. These newly developed and well-characterized models are expected to serve as valuable platforms for accelerating the development of novel therapeutic strategies for ATC.

INTRODUCTION

Anaplastic thyroid carcinoma (ATC) is one of the most aggressive human malignancies, with a reported median overall survival (OS) of approximately 3 to 6 months, and it remains associated with an extremely poor prognosis [1, 2]. Although a recent study reported the clinical efficacy of tyrosine kinase inhibitors in treating ATC [3], some studies have shown that patients with *BRAF* V600E–mutated ATC have better outcomes when treated with BRAF inhibitors [4, 5]. Despite these therapeutic advances, however, ATC continues to have high mortality, and more effective treatment strategies are urgently needed.

Although several preclinical studies have evaluated therapeutic efficacy in vivo using ATC-derived cell line–based animal models [6–8], a major limitation of such models is the loss of intratumoral heterogeneity that occurs during the establishment and long-term propagation of cancer cell lines [9]. Patient-derived xenograft (PDX) models—which are thought to better preserve the original tumor architecture, molecular characteristics, and tumor microenvironment—have been increasingly utilized to overcome this limitation [10]. Several studies have successfully established PDX models for ATC [11–13], but the number of available models remains limited. Various PDX models have been established at Kumamoto University using Balb/c $Rag2^{-/-}Jak3^{-/-}$ (BRJ) mice [10, 14]. In the present study, we established a novel ATC cell line and corresponding novel PDX model harboring the *BRAF* V600E mutation.

MATERIALS AND METHODS

Patient

An 89-year-old woman who had undergone a right thyroid lobectomy 30 years earlier was referred to Kumamoto University Hospital due to sudden anterior neck swelling. Although details of her previous thyroid surgery were unknown, and no medical records were available, the patient reported that her attending physician had informed her that the tumor was benign. Computed tomography (CT) scan revealed a 33-mm mass in the thyroid isthmus, with suspected invasion of the anterior tracheal wall. Fine-needle aspiration cytology suggested ATC. Consequently, total thyroidectomy and tracheal window resection with tracheocutaneous fistula creation were performed 2 weeks after initial presentation. The final pathology report confirmed the diagnosis as ATC derived from papillary thyroid carcinoma (PTC). Figure 1 shows the pre- and postoperative CT scans and hematoxylin and eosin (H&E)-stained sections of the surgical specimen.

Cell line establishment

Primary ATC tissues obtained during the surgery were minced into small fragments using sterile scissors. The tissue samples were then enzymatically dissociated by treatment with collagenase I (Cat#031-17601; Fujifilm Wako Pure Chemical, Osaka, Japan) and dispase II (Cat#17105041; Gibco, Thermo Fisher Scientific, Grand Island, NY, USA) for 60 min at 37°C. The resulting cell suspension was seeded onto 60-mm tissue culture dishes and maintained in Dulbecco's Modified Eagle Medium/Ham's F-12 with L-glutamine and phenol red (DMEM/F-12; Cat#048-29785; Fujifilm Wako Pure Chemical), supplemented with 10% heat-inactivated fetal bovine serum (FBS; Sigma-Aldrich, St. Louis, MO, USA) and 1% penicillin-streptomycin (100 U/mL penicillin and 100 µg/mL streptomycin). Cultures were incubated at 37°C in a humidified atmosphere with 5% CO_2, and the medium was replaced every 3–4 days. After > 6 months of continuous culture, a stable cell line was successfully established and designated as OK (Otolaryngology Kumamoto)-ATC1. For long-term maintenance, OK-ATC1 cells were cultured in Dulbecco's Modified Eagle Medium (High Glucose) with L-glutamine and phenol red (DMEM; Cat# 044-29765, Fujifilm Wako Pure Chemical), supplemented with 10% FBS and 1% penicillin-streptomycin.

DNA extraction and short tandem repeat (STR) analysis

Genomic DNA was extracted from OK-ATC1 cells in the logarithmic growth phase and from patient-derived peripheral blood mononuclear cells (PBMCs) using Proteinase K (Cat#9034, TaKaRa Bio Inc., Shiga, Japan) according to the manufacturer's instructions. To exclude potential cross-contamination during culture and verify the genetic identity between the patient and OK-ATC1 cell line, the extracted DNA samples were STR profiled by BEX Corporation (Tokyo, Japan). STR analysis was performed using the GenePrint®10 system (Promega, Madison, WI, USA).

Mycoplasma contamination inspection

Mycoplasma contamination was evaluated using a MycoAlert™ *Mycoplasma* Detection kit (Cat#LT37-618, Lonza, Rockland, ME, USA) according to the manufacturer's instructions. Bioluminescence was

measured using a multi-mode microplate reader (SpectraMax i3x; Molecular Devices, San Jose, CA, USA). OK-ATC1 cells were confirmed as *Mycoplasma*-free (ratio < 0.9) before use in experiments.

Cell proliferation assay

Cell proliferation was assessed using a Cell Counting Kit-8 (CCK-8; Cat#343–07623, Dojindo Molecular Technologies, Kumamoto, Japan) according to the manufacturer's instructions. Briefly, OK-ATC1 cells were seeded in triplicate in 96-well flat-bottom plates at a density of 5.0×10^3 cells/well. After incubation for 24, 48, 72, and 96 h, CCK-8 solution was added to each well at a final concentration of 0.5 mg/mL. The plates were then incubated for an additional 2 h, and the optical density was measured at 450 nm using a Multiskan FC microplate reader (Thermo Fisher Scientific, Waltham, MA, USA). Graphical plots were generated using Microsoft Excel for Microsoft 365 (version 2608, 64-bit; Microsoft Corp., Redmond, WA, USA). Cell doubling time was calculated using an online Cell Doubling Time Calculator (Omni Calculator; https://www.omnicalculator.com/biology/cell-doubling-time).

Establishment of the PDX model

Primary ATC tumor blocks were collected from resected tumor tissues and cut into 5-mm pieces with scissors in medium. The dissected tissues were implanted in the flanks of 6- to 12-week-old female BRJ mice provided by the Center for Human Retrovirus Research Department of Hematology and Oncology, Kumamoto University, under general anesthesia with isoflurane (founder generation: F0). Following transplantation, the health of the mice was assessed once weekly at the Center for Animal Resources and Development, Kumamoto University.

Mice were euthanized when the tumor major axis reached approximately 1 cm. Tumors were excised (referred to as passage 1; p1), mechanically minced, and transplanted into the flanks of the next cohort of BRJ mice at a 1:5 ratio to generate the F1 generation. Tumors were serially passaged up to generation F3. Tumor fragments from generations F0–F3 were utilized for multiple purposes: subsequent transplantation into the next cohort, snap-freezing in liquid nitrogen for STR analysis, or formalin-fixation for histological evaluation. For long-term cryopreservation, additional fragments were stored in BAMBANKER™ (Cat#CS-02-002, GC Lymphotec Inc., Tokyo, Japan). The resulting tumors harvested from F3 mice (referred to as passage 4; p4) were then processed for analysis: one half of each tumor was fixed in 4% paraformaldehyde and embedded in paraffin for immunohistochemistry (IHC) analysis, whereas the other half was preserved for genetic analysis.

The PDX model was considered successfully established when tumors were serially expanded from F0 to F3 (a total of four generations) and when re-engraftment was achievable from cryopreserved tumor samples. The established PDX model was designated OK-ATC1-PDX.

Histological analysis of tumor tissue

Histological examinations were performed on clinical formalin-fixed paraffin-embedded (FFPE) tissues, OK-ATC1 cell blocks, and OK-ATC1-PDX samples. The samples were sectioned at a thickness of 4 μm, followed by deparaffinization and H&E staining according to standard protocols.

IHC analysis

IHC analyses were also performed on clinical FFPE tissues, OK-ATC1 cell blocks, and OK-ATC1-PDX samples. Tissue sections (4 μm thick) were deparaffinized with xylene and rehydrated using graded ethanol. After antigen retrieval, endogenous peroxidase activity was quenched with 1% hydrogen peroxide in absolute methanol for 30 min. Following blocking with 5% goat serum in phosphate-buffered saline for 20 min, sections were incubated overnight with primary antibodies at 4°C. The next day, sections were incubated with a horseradish peroxidase–conjugated secondary antibody at room temperature for 30 min. Detection was carried out using diaminobenzidine as the chromogen. Finally, all slides were counterstained with hematoxylin for 20 s, dehydrated, and cover-slipped for evaluation. The Ki-67 index was calculated using HALO® software (Indica Labs; distributed by Visualix, Kobe, Japan).

BRAF inhibitor in vitro susceptibility assay

OK-ATC1 cells in logarithmic growth phase were diluted in culture medium to a density of 2×10^4 cells/mL. A 100-μL aliquot of the cell suspension was seeded into each well of a 96-well plate, which was incubated for 24 h at 37°C in a humidified atmosphere containing 5% CO_2. Subsequently, three BRAF inhibitors—dabrafenib (Cat#S2807), encorafenib (Cat#S7108), and vemurafenib (Cat#S1267; all from Selleck Biotechnology, Kanagawa, Japan)—were serially diluted in culture medium to achieve a concentration in the range 0.0002 to 200 μM. A 100-μL volume of each diluted drug solution was added to the respective wells, and the plate was incubated for an additional 72 h under the same conditions. After incubation, 100 μL of culture medium was aspirated from each well using an 8-channel pipette, and 10 μL of CCK-8 solution was added. Following a 2-h incubation at 37°C, the absorbance of each well at 450 nm was measured using a microplate reader. The data were analyzed using GraphPad Prism software (version 11.1.0 for Mac, GraphPad Software, Boston, MA, USA) to calculate half-maximal inhibitory concentration (IC_{50}) values. Two types of control wells were prepared: untreated control wells containing cells in culture medium without any drug (representing 100% cell viability) and blank control wells containing culture medium alone.

Genetic mutation analysis

In Japan, comprehensive genomic profiling tests are approved for ATC and other thyroid malignancies when standard treatments are no longer effective or feasible. For the clinical specimen, genetic mutation data were derived from the FoundationOne® CDx (Chugai Pharmaceutical Co., Ltd., Tokyo, Japan) analysis conducted during the course of standard clinical treatment. Based on the results, we analyzed genetic mutations in OK-ATC1 and OK-ATC1-PDX—specifically *BRAF* V600E, *TP53* V73fs*50, and

telomerase reverse transcriptase (*TERT*) promoter − 146C > T—using Sanger sequencing (FASMAC, Kanagawa, Japan). The primer sequences, which were based in part on previous reports [15, 16], are shown in Supplementary Table S3. Sanger sequencing data were analyzed using SnapGene software (version 8.2.3; Dotmatics, Boston, MA, USA).

RESULTS

Clinical and pathological features of the patient

The ATC diagnosis for this patient was confirmed based on permanent histopathological specimens. Postoperative CT revealed multiple disseminated pulmonary metastases. To identify potential therapeutic targets, a genetic analysis was performed using Oncomine™ Dx Target Test (SRL, Japan), a next-generation sequencing assay, which identified a *BRAF* V600E mutation. Although combination therapy with encorafenib and binimetinib was initiated, the treatment was discontinued due to intolerable adverse effects, including diarrhea and visual impairment. Treatment was switched to low-dose lenvatinib. However, a CT scan performed 5 months after lenvatinib initiation revealed progression of the lung metastases and a new left adrenal metastasis. FoundationOne® CDx testing identified *BRAF* V600E, *TERT* promoter − 146C > T, *TP53* V73fs*50, and additional mutations (Supplementary Table S1).

Establishment of a novel cell line derived from ATC tissue

A novel cell line, designated OK-ATC1, was established from the primary tumor tissue of this patient. OK-ATC1 cells remained adherent during culture proliferation for > 6 months without detectable *Mycoplasma* contamination. Cell line authentication via 10-locus STR profiling confirmed a 100% match between OK-ATC1 cells and the patient's PBMCs (Supplementary Table S2). These results confirmed successful establishment of the OK-ATC1 cell line from this ATC patient. The STR profile of the established cell line was compared with known human cell lines using the Cellosaurus database (CLASTR tool). No matching cell lines were identified using the Masters algorithm (threshold 80%), confirming the uniqueness of the cell line and the absence of cross-contamination with common laboratory cell lines. Thus, OK-ATC1 is a novel ATC cell line.

OK-ATC1 cells exhibited a spindle-shaped morphology (Fig. 2a) and grew adhesively, with a doubling time of 30 h 6.3 min (Fig. 2b). Cells could be recovered after freezing in medium at − 80°C and subsequent thawing.

Establishment of a novel PDX model

A 10-mm-square tissue piece was harvested from the tumor region of the patient's resected surgical specimen, and a PDX model, designated OK-ATC1-PDX, was established using the method described above. Once the major tumor diameter exceeded 1 cm, the mice were euthanized, and tumors were harvested. The time intervals required for tumors to reach the predetermined size were 28 days for

passage 1 (p1), 21 days from p1 to p2, 15 days from p2 to p3, and 14 days from p3 to p4. Figure 3 shows representative images of p4.

Histological and immunophenotypic characterization of clinical-FFPE, cell block, and PDX samples

FFPE clinical tissue sections containing both PTC and ATC components within the same section were utilized. Results of comparative IHC analyses of the clinical PTC and ATC components, cell block of OK-ATC1 (cell block), and OK-ATC1-PDX (PDX) are shown in Figs. 4 and 5. Table 1 provides detailed interpretations of these findings. Table 2 lists the antibodies used.

Table 1
Evaluation of immunohistochemical staining.

	Clinical-FFPE		**OK-ATC1**	**OK-ATC1-PDX**
	PTC	**ATC**	**Cell block**	**p4**
AE1/AE3	+	+	+	+
p53	+	-	-	-
PAX8	+	+	+	+
TTF-1	+	-	-	-
Ki-67	+	+	+	+
BRAF	+	+	+	+
TGF-β	-	+	-	+
PMS2	+	+	+	+
MSH6	+	+	+	+
PD-L1	-	+	+	+

Summary of immunohistochemical evaluations. Staining characteristics of the cell blocks and PDX models closely recapitulated those of the clinical ATC component. PTC: papillary thyroid carcinoma, ATC: anaplastic thyroid carcinoma

Table 2
Antibodies for immunohistochemical staining

Primary antibody	Manufacturer	Catalog Number
AE1/AE3	DAKO	IR053
p53	DAKO	M7001
PAX8	Nichirei Biosciences	418391
TTF-1	DAKO	N1635
Ki-67	DAKO	M7240
BRAF	Roche	518-115142
TGF-β	R&D Systems	MAB1835
PMS2	DAKO	IR087
MSH6	DAKO	IR086
PD-L1	DAKO	22C3
COX-IV	Cell Signaling	#4850

IHC revealed that all samples were positive for both AE1/AE3 and PAX8. By contrast, the clinical PTC component was positive for p53 and TTF-1, whereas the clinical ATC component, cell block, and PDX were negative. The Ki-67 index, determined using HALO® software, was low in the PTC component, at 6.46%, but markedly elevated in the ATC component (54.69%), cell block (82.75%), and PDX (80.11%). These findings demonstrated distinct differences in cytological features and proliferative capacity among the components while confirming that the established cell block and PDX model largely recapitulate the aggressive phenotype of the clinical ATC component. Furthermore, cytochrome c oxidase polypeptide IV immunostaining was positive in both the cell block and PDX tissues, verifying the human origin of these established models (Supplementary Fig. S1).

Evaluation of therapeutic targets and microenvironmental markers

Molecular profiles potentially relevant to therapeutic efficacy and the tumor microenvironment were evaluated by analyzing the expression patterns of BRAF, TGF-β, PMS2, MSH6, and PD-L1 (Fig. 5). BRAF staining was faintly positive in the PTC component and slightly stronger in the ATC component, but it exhibited diffuse, strong staining in both the cell block and PDX. TGF-β staining was extremely focal in the clinical PTC component and cell block but faint and widespread in both the clinical ATC component and PDX. Regarding mismatch repair (MMR) status, both PMS2 and MSH6 demonstrated nuclear positivity across all tested specimens. Although PMS2 staining was relatively faint in the PTC component compared with other components, MSH6 showed diffuse nuclear positivity in all specimens, with additional cytoplasmic staining observed uniquely in the PDX. PD-L1 expression was negligible in

the PTC component; however, diffuse and robust positivity was observed in the ATC component, cell block, and PDX. These data suggest that the newly established OK-ATC1 cell line and OK-ATC1-PDX model efficiently preserve the immunotherapeutic and molecular therapeutic target profiles characteristic of advanced clinical ATC.

Sensitivity of OK-ATC1 cells to BRAF inhibitors

Figure 6 shows the results of in vitro drug sensitivity assays of OK-ATC1 cells treated with the BRAF inhibitors dabrafenib, encorafenib, and vemurafenib. The IC_{50} values were 45.1 μM for dabrafenib, 5.1 μM for encorafenib, and 9.9 μM for vemurafenib. Notably, for dabrafenib, cell survival was reduced to only approximately 50% even at a high concentration of 100 μM.

Verification of BRAF, TP53, and TERT Promoter Mutations in OK-ATC1 and OK-ATC1-PDX

Sanger sequencing chromatograms confirming the genomic variants are shown in Fig. 7. Consistent with the findings from the primary tumor tissue, both OK-ATC1 cells and the OK-ATC1-PDX model harbored heterozygous *BRAF* V600E and *TERT* promoter − 146C > T mutations, as well as a *TP53* V73fs*50 mutation. The corresponding antisense strand sequencing chromatograms are shown in Supplementary Fig. S2.

DISCUSSION

Genetic alterations in ATC

ATC is thought to arise from differentiated thyroid carcinoma through the accumulation of multiple genetic alterations, including gene mutations and deletions, leading to tumor dedifferentiation [17–19]. *BRAF* V600E is the most frequent mutation observed in PTC, and this mutation is also reported in approximately 25–45% of ATC cases. Other representative genetic alterations in ATC include *TP53* mutations (65–80%), *TERT* promoter mutations (65–73%), *RAS* family mutations (*KRAS*, *NRAS*, *HRAS*; 20–30%), *PIK3CA* mutations (14–25%), and *PTEN* deletions (10–20%), among others [6, 13, 18–21]. In a large-scale genetic analysis of 779 advanced thyroid cancer cases, Pozdeyev et al. demonstrated that *BRAF* V600E mutations in ATC are predominantly associated with progression from PTC, whereas *RAS* mutations are more frequent in cases arising from follicular-patterned tumors [21]. Furthermore, model mice harboring the *Braf* V600E mutation in combination with either *Pik3ca* H1047R or *Tp53* R270H mutations reportedly develop ATC [18, 22]. These findings underscore that the pathogenesis of ATC is driven by the synergistic accumulation of multiple genetic alterations.

The pathological findings in this case were suggestive of ATC arising from PTC, consistent with the presence of the *BRAF* V600E mutation. These results are in agreement with previous reports.

Immunohistochemical validation of OK-ATC1 and OK-ATC1-PDX

The diagnosis of ATC generally relies on a combination of H&E-stained morphology and a comprehensive IHC profile, as there are no specific diagnostic protein markers. Accordingly, we curated our IHC markers based on established reports from the ATC Research Consortium of Japan by Hirokawa et al. [2], as well as the study by Maniakas et al. [12].

First, the staining patterns of key diagnostic markers, such as p53 and TTF-1, closely recapitulated those observed in the clinical ATC component in both the OK-ATC1 cell block and PDX, supporting the conclusion that both OK-ATC1 and OK-ATC1-PDX were successfully derived from the ATC fraction of the primary tumor. The Ki-67 index was higher in the cell block and PDX than the clinical specimen; however, such accelerated cell proliferation would be expected given the optimized in vitro culture conditions and immunodeficient environment in vivo, respectively. Regarding potential therapeutic targets and microenvironmental markers, BRAF positivity was consistently demonstrated across all specimens by IHC, which aligned perfectly with our Sanger sequencing results. Intriguingly, TGF-β expression was decreased in the cell block compared to both the clinical ATC component and PDX. This variation suggests that TGF-β expression is influenced by the tumor microenvironment and that the in vitro cell line model may have certain limitations as a platform for developing TGF-β–targeted therapeutics. Furthermore, the MMR proteins PMS2 and MSH6 retained nuclear expression in both the cell block and PDX, consistent with clinical FFPE findings. This preserved MMR proficiency is highly consistent with the microsatellite-stable phenotype identified by the clinical FoundationOne® CDx assay. Finally, although PD-L1 expression was completely absent in the clinical PTC component, robust and diffuse PD-L1 positivity was observed in the ATC component, cell block, and PDX. These findings further confirm that OK-ATC1 and OK-ATC1-PDX faithfully preserve the immunophenotypic and microenvironmental characteristics of the advanced clinical ATC component.

Review of the literature regarding ATC PDX models

Table 3 summarizes previous reports on the simultaneous establishment of ATC cell lines and PDX models alongside our current findings. Marlow et al. suggested that the presence of a *TERT* promoter mutation could be predictive of successful PDX establishment [13]. This scenario is highly plausible, considering that *TERT* promoter mutations are detected in only 9% of PTC cases but increase to 40% in poorly differentiated thyroid carcinomas and up to 73% in ATC, with mutation-positive cases strongly associated with a poor prognosis [20]. This is further supported by evidence indicating a higher success rate for PDX establishment with more aggressive tumors [10]. Among mutations, the *TERT* promoter −146C > T mutation is the second most common variant after the predominant −124C > T (C228T) mutation, occurring in approximately 6% of ATC cases [20]. To our knowledge, no previous studies that simultaneously established both an ATC cell line and PDX model have reported a *TERT* promoter −146C > T mutation, highlighting the unique value and scarcity of our newly developed PDX model. In the present case, the *TERT* promoter −146C > T mutation was identified in the clinical specimen, suggesting that although this tumor exhibited characteristics favorable for PDX establishment, it unfortunately also signified a highly aggressive disease with an unfavorable prognosis.

Table 3
Summary of established both of cell lines and patient-derived xenograft (PDX) models of anaplastic thyroid carcinoma (ATC)

Reference	Cell lines		PDX models		Patient Tumor Mutations
	Name	Mutations	Name	Mutations	
Schweppe et al. (2019) [11]	CUTC60	BRAF V600E, TP53 H193R, TERT promoter − 124C > T	CUTC60-PDX	BRAF V600E, TP53 H193R, TERT promoter − 124C > T	Not available
Maniakas et al. (2021) [12]	MDA-T187	BRAF V600E, TP53 K132N	MDA-ATC1	BRAF V600E, TP53 K132N	BRAF V600E
	MDA-T248	BRAF V600E, TP53 c.994-1G > C, CDKN2A D74N	MDA-ATC4	BRAF V600E, TP53 R280T, CDKN2A D74N	BRAF V600E, TP53 R280T, CDKN2A D74N
	MDA-T269	TERT promoter (-124C > T), HRAS G13R	MDA-ATC5	TERT promoter (-124C > T), HRAS G13R	TERT promoter (-124C > T), HRAS G13R
	MDA-T273	TERT promoter (-124C > T), KRAS G12R, TP53 R175H, NFE2L2 D27Y	MDA-ATC6	TERT promoter (-124C > T), KRAS G12R, TP53 R175H, NFE2L2 D27Y	TERT promoter (-124C > T), KRAS G12R, TP53 (R175H, G244fs*, c.783-1G > T), NF2 E317*, NFE2L2 D27Y
Marlow et al. (2018) [13]	JEM493	HRAS Q61R, TERT promoter C228T	MC-Th-493	HRAS Q61R, TERT promoter C228T	Not available
	THJ560	BRAF V600E, TP53 V274F, TERT promoter (C228T, T349C)	MC-Th-560	BRAF V600E, TP53 V274F, TERT promoter (C228T, T349C)	Not available
Our case	OK-ATC1	BRAF V600E, TP53 V73fs*50, TERT promoter − 146C > T	OK-ATC1-PDX	BRAF V600E, TP53 V73fs*50, TERT promoter − 146C > T	BRAF V600E, TP53 V73fs*50, TERT promoter − 146C > T, among others*

*Detailed information, including other genetic mutations, is provided in Supplementary Table S1.

Response to BRAF inhibitor treatment

The OK-ATC1 cell line newly established in this study demonstrated an IC_{50} range of 5.1–45.1 μM for BRAF inhibitor monotherapy. Although the high sensitivity of melanoma cell lines to single-agent BRAF

inhibitor treatment is well-documented, with IC_{50} values typically < 1 μM [23, 24], thyroid cancer cells frequently exhibit a much higher resistance profile. For instance, vemurafenib reportedly exhibits elevated IC_{50} values in thyroid cancer, ranging from 27.60 to 48.73 μM. This therapeutic resistance is largely attributed to the relief of ERK-mediated negative feedback inhibition upon BRAF blockade, which triggers the rapid compensatory reactivation of multiple receptor tyrosine kinases, such as EGFR and HER3 [25]. Furthermore, previous literature indicated that BRAF inhibitor monotherapy exerts limited tumor-suppressive effects in ATC, but combined treatment with a MEK inhibitor significantly enhances tumor shrinkage. However, even this combination therapy fails to completely eradicate cancer stem cells, which potentially serve as a reservoir for recurrence and treatment resistance [26]. Although combination therapies were not evaluated in our study, our results suggest that despite harboring the *BRAF* mutation, OK-ATC1 cells exhibit a clear resistance profile to BRAF inhibitor monotherapy, consistent with previously reported ATC cell lines.

A meta-analysis of BRAF/MEK inhibitor therapy in *BRAF* V600E-mutant ATC reported an OS of 14.5 months, with 1-year and 2-year survival rates of 64.97% and 52.08%, respectively. Among patients receiving BRAF/MEK inhibitors, those who underwent neoadjuvant therapy achieved significantly better 1-year and 2-year OS rates compared with those treated at other time points [27]. Although these outcomes represent a remarkable prognostic improvement compared with the historical median OS of only 3–6 months, ATC undeniably remains a highly lethal disease with an unfavorable prognosis. We hope that the novel cell line and PDX model established in this study will serve as valuable tools in the development of further therapeutic strategies.

Limitations

This study has several limitations. First, because our findings are based on a cell line established from only a single case, the overall success rate of ATC PDX model establishment in BRJ mice remains unknown. Second, genetic analyses of the cell line and PDX model were performed using Sanger sequencing, which does not comprehensively capture all genetic alterations across the genome. Finally, regarding therapeutic responses, the efficacy of combining a BRAF inhibitor with an MEK inhibitor was not evaluated and thus remains undetermined.

DECLARATIONS

Conflicts of interest:

The authors declare that they have no conflicts of interest.

Ethical approval and consent to participate:

The study protocols were approved by the Institutional Review Board of the Kumamoto University Faculty of Life Science Ethnics Committee (Genome #593, 2024, 22 November), and the study was performed in

line with the principles of the Declaration of Helsinki. The animal study protocols were also approved by the Institutional Review Board of Kumamoto University (A2024-076R1, 2025, 20 January, and A2026-020, 2026, 1 June) and experiments were performed in accordance with the animal handling guidelines of Kumamoto University.

Informed consent:

Informed consent was obtained from the donor.

Funding:

This work was supported by grants from the Japan Society for the Promotion of Science (JSPS) KAKENHI (number JP24K12720 [to YO]) and The Soda Toyoji Memorial Foundation.

ACKNOWLEDGEMENTS

We would like to express our sincere gratitude to the staff of the Department of Otolaryngology–Head and Neck Surgery at Kumamoto University Hospital for their dedicated clinical care of this patient. We are also deeply grateful to the members of the Division of Hematopoiesis Joint Research Center for Human Retrovirus Infection, and the Department of Cell Pathology at Kumamoto University, for their invaluable guidance in experimental techniques and for providing the experimental animals used in this study. The authors thank FORTE Science Communications (https://www.forte-science.co.jp/) for English language editing.

AUTHOR CONTRIBUTIONS

Yu Shimoda: Tissue sample collection and cell/tissue management, histological and immunohistochemical analyses, and drafting of the manuscript; Yukio Fujiwara and Yoshihiro Komohara: Immunohistochemical staining and supervision of result interpretation; Winidmanokul Peeranut and Hiromi Aoki: Establishment and maintenance of the cell line and PDX model; Kaori Yukino and Akira Murakami: Maintenance of the cell line; Haruki Saito: Technical guidance on experimental procedures; Seiji Okada: Establishment and management of the cell line and PDX model, and supervision of experimental techniques; Yorihisa Orita: Supervision of the entire study. All authors approved the final manuscript.

REFERENCES

1. Lin B, Ma H, Ma M, Zhang Z, Sun Z, Hsieh I et al. The incidence and survival analysis for anaplastic thyroid cancer: a SEER database analysis.
2. Hirokawa M, Sugitani I, Kakudo K, Sakamoto A, Higashiyama T, Sugino K, et al. Histopathological analysis of anaplastic thyroid carcinoma cases with long-term survival: A report from the Anaplastic

Thyroid Carcinoma Research Consortium of Japan. Endocr J. 2016;63:441–7. https://doi.org/10.1507/endocrj.EJ15-0705.

3. Tahara M, Kiyota N, Yamazaki T, Chayahara N, Nakano K, Inagaki L, et al. Lenvatinib for Anaplastic Thyroid Cancer. Front Oncol [Internet]. 2017. https://doi.org/10.3389/fonc.2017.00025. [cited 2026 Jan 12];7.
4. Wang JR, Montierth M, Xu L, Goswami M, Zhao X, Cote G, et al. Impact of Somatic Mutations on Survival Outcomes in Patients With Anaplastic Thyroid Carcinoma. JCO Precis Oncol. 2022;e2100504. https://doi.org/10.1200/PO.21.00504.
5. Zhao X, Wang JR, Dadu R, Busaidy NL, Xu L, Learned KO, et al. Surgery After BRAF-Directed Therapy Is Associated with Improved Survival in $BRAF^{V600E}$ Mutant Anaplastic Thyroid Cancer: A Single-Center Retrospective Cohort Study. Thyroid. 2023;33:484–91. https://doi.org/10.1089/thy.2022.0504.
6. ElMokh O, Taelman V, Radojewski P, Roelli MA, Stoss A, Dumont RA, et al. MEK Inhibition Induces Therapeutic Iodine Uptake in a Murine Model of Anaplastic Thyroid Cancer. J Nucl Med. 2019;60:917–23. https://doi.org/10.2967/jnumed.118.216721.
7. Gunda V, Gigliotti B, Ndishabandi D, Ashry T, McCarthy M, Zhou Z, et al. Combinations of BRAF inhibitor and anti-PD-1/PD-L1 antibody improve survival and tumour immunity in an immunocompetent model of orthotopic murine anaplastic thyroid cancer. Br J Cancer. 2018;119:1223–32. https://doi.org/10.1038/s41416-018-0296-2.
8. Diaz D, Bergdorf K, Loberg MA, Phifer CJ, Xu GJ, Sheng Q, et al. Wnt/β-catenin signaling is a therapeutic target in anaplastic thyroid carcinoma. Endocrine. 2024;86:114–8. https://doi.org/10.1007/s12020-024-03887-0.
9. Abdolahi S, Ghazvinian Z, Muhammadnejad S, Saleh M, Asadzadeh Aghdaei H, Baghaei K. Patient-derived xenograft (PDX) models, applications and challenges in cancer research. J Transl Med. 2022;20:206. https://doi.org/10.1186/s12967-022-03405-8.
10. Okada S, Vaeteewoottacharn K, Kariya R. Application of Highly Immunocompromised Mice for the Establishment of Patient-Derived Xenograft (PDX) Models. Cells MDPI AG. 2019;8:889. https://doi.org/10.3390/cells8080889.
11. Schweppe RE, Pozdeyev N, Pike LA, Korch C, Zhou Q, Sams SB, et al. Establishment and Characterization of Four Novel Thyroid Cancer Cell Lines and PDX Models Expressing the RET/PTC1 Rearrangement, BRAFV600E, or RASQ61R as Drivers. Mol Cancer Res. 2019;17:1036–48. https://doi.org/10.1158/1541-7786.MCR-18-1026.
12. Maniakas A, Henderson YC, Hei H, Peng S, Chen Y, Jiang Y, et al. Novel Anaplastic Thyroid Cancer PDXs and Cell Lines: Expanding Preclinical Models of Genetic Diversity. J Clin Endocrinol Metab. 2021;106:e4652–65. https://doi.org/10.1210/clinem/dgab453.
13. Marlow LA, Rohl SD, Miller JL, Knauf JA, Fagin JA, Ryder M, et al. Methodology, Criteria, and Characterization of Patient-Matched Thyroid Cell Lines and Patient-Derived Tumor Xenografts. J Clin Endocrinol Metab. 2018;103:3169–82. https://doi.org/10.1210/jc.2017-01845.

14. Ono A, Hattori S, Kariya R, Iwanaga S, Taura M, Harada H et al. Comparative Study of Human Hematopoietic Cell Engraftment into Balb/c and C57BL/6 Strain of Rag-2/Jak3 Double-Deficient Mice. Ahmad N, editor. BioMed Res Int [Internet]. Wiley; 2011 [cited 2025 May 23];2011. https://doi.org/10.1155/2011/539748
15. Henderson YC, Shellenberger TD, Williams MD, El-Naggar AK, Fredrick MJ, Cieply KM, et al. High Rate of BRAF and RET/PTC Dual Mutations Associated with Recurrent Papillary Thyroid Carcinoma. Clin Cancer Res. 2009;15:485–91. https://doi.org/10.1158/1078-0432.CCR-08-0933.
16. Panebianco F, Nikitski AV, Nikiforova MN, Nikiforov YE. Spectrum of *TERT* promoter mutations and mechanisms of activation in thyroid cancer. Cancer Med. 2019;8:5831–9. https://doi.org/10.1002/cam4.2467.
17. Nikiforova MN, Kimura ET, Gandhi M, Biddinger PW, Knauf JA, Basolo F, et al. BRAF Mutations in Thyroid Tumors Are Restricted to Papillary Carcinomas and Anaplastic or Poorly Differentiated Carcinomas Arising from Papillary Carcinomas. J Clin Endocrinol Metab. 2003;88:5399–404. https://doi.org/10.1210/jc.2003-030838.
18. Charles R-P, Silva J, Iezza G, Phillips WA, McMahon M. Activating BRAF and PIK3CA Mutations Cooperate to Promote Anaplastic Thyroid Carcinogenesis. Mol Cancer Res. 2014;12:979–86. https://doi.org/10.1158/1541-7786.MCR-14-0158-T.
19. Kunstman JW, Juhlin CC, Goh G, Brown TC, Stenman A, Healy JM, et al. Characterization of the mutational landscape of anaplastic thyroid cancer via whole-exome sequencing. Hum Mol Genet. 2015;24:2318–29. https://doi.org/10.1093/hmg/ddu749.
20. Landa I, Ibrahimpasic T, Boucai L, Sinha R, Knauf JA, Shah RH, et al. Genomic and transcriptomic hallmarks of poorly differentiated and anaplastic thyroid cancers. J Clin Invest. 2016;126:1052–66. https://doi.org/10.1172/JCI85271.
21. Pozdeyev N, Gay LM, Sokol ES, Hartmaier R, Deaver KE, Davis S, et al. Genetic Analysis of 779 Advanced Differentiated and Anaplastic Thyroid Cancers. Clin Cancer Res. 2018;24:3059–68. https://doi.org/10.1158/1078-0432.CCR-18-0373.
22. McFadden DG, Vernon A, Santiago PM, Martinez-McFaline R, Bhutkar A, Crowley DM, et al. p53 constrains progression to anaplastic thyroid carcinoma in a *Braf* -mutant mouse model of papillary thyroid cancer. Proc Natl Acad Sci [Internet]. 2014. https://doi.org/10.1073/pnas.1404357111. [cited 2026 Jan 12];111.
23. Koelblinger P, Thuerigen O, Dummer R. Development of encorafenib for BRAF-mutated advanced melanoma. Curr Opin Oncol. 2018;30:125–33. https://doi.org/10.1097/CCO.0000000000000426.
24. Lassen A, Atefi M, Robert L, Wong DJ, Cerniglia M, Comin-Anduix B, et al. Effects of AKT inhibitor therapy in response and resistance to BRAF inhibition in melanoma. Mol Cancer. 2014;13:83. https://doi.org/10.1186/1476-4598-13-83.
25. Ma W, Tian M, Hu L, Ruan X, Zhang W, Zheng X, et al. Early Combined SHP2 Targeting Reverses the Therapeutic Resistance of Vemurafenib in Thyroid Cancer. J Cancer. 2023;14:1592–604. https://doi.org/10.7150/jca.83853.

26. Kimura T, Doolittle WKL, Kruhlak M, Zhao L, Hwang E, Zhu X et al. Inhibition of MEK Signaling Attenuates Cancer Stem Cell Activity in Anaplastic Thyroid Cancer. Thyroid®. 2024;thy.2023.0521. https://doi.org/10.1089/thy.2023.0521
27. Priantti JN, Rodrigues NMV, De Moraes FCA, Da Costa AG, Jezini DL, Heckmann MIO. Efficacy and safety of BRAF/MEK inhibitors in BRAFV600E-mutated anaplastic thyroid cancer: a systematic review and meta-analysis. Endocrine. 2024;86:284–92. https://doi.org/10.1007/s12020-024-03845-w.
28. Okada T, Nakamura T, Watanabe T, Onoda N, Ashida A, Okuyama R et al. Coexpression of EpCAM, CD44 Variant Isoforms and Claudin-7 in Anaplastic Thyroid Carcinoma. Izumi H, editor. PLoS ONE. 2014;9:e94487. https://doi.org/10.1371/journal.pone.0094487
29. Lundgren Mortensen AC, Berglund H, Jha P, Stenman A, Selvaraju RK, Lundqvist H, et al. Dual-Nuclide Biodistribution and Therapeutic Evaluation of a Novel Antibody-Based Radiopharmaceutical in Anaplastic Thyroid Cancer Xenografts. Mol Cancer Ther. 2025;24:753–62. https://doi.org/10.1158/1535-7163.MCT-24-0524.
30. Mortensen ACL, Imgenberg-Kreuz J, Spiegelberg D, Botling J, Nestor M. Utilizing CD44v6 and V600EBRAF-mutation for in vitro targeted combination therapy of thyroid carcinomas. Heliyon. 2023;9:e22594. https://doi.org/10.1016/j.heliyon.2023.e22594.
31. Kinugasa Y, Matsui T, Takakura N. CD44 Expressed on Cancer-Associated Fibroblasts Is a Functional Molecule Supporting the Stemness and Drug Resistance of Malignant Cancer Cells in the Tumor Microenvironment. Stem Cells. 2014;32:145–56. https://doi.org/10.1002/stem.1556.

Figures

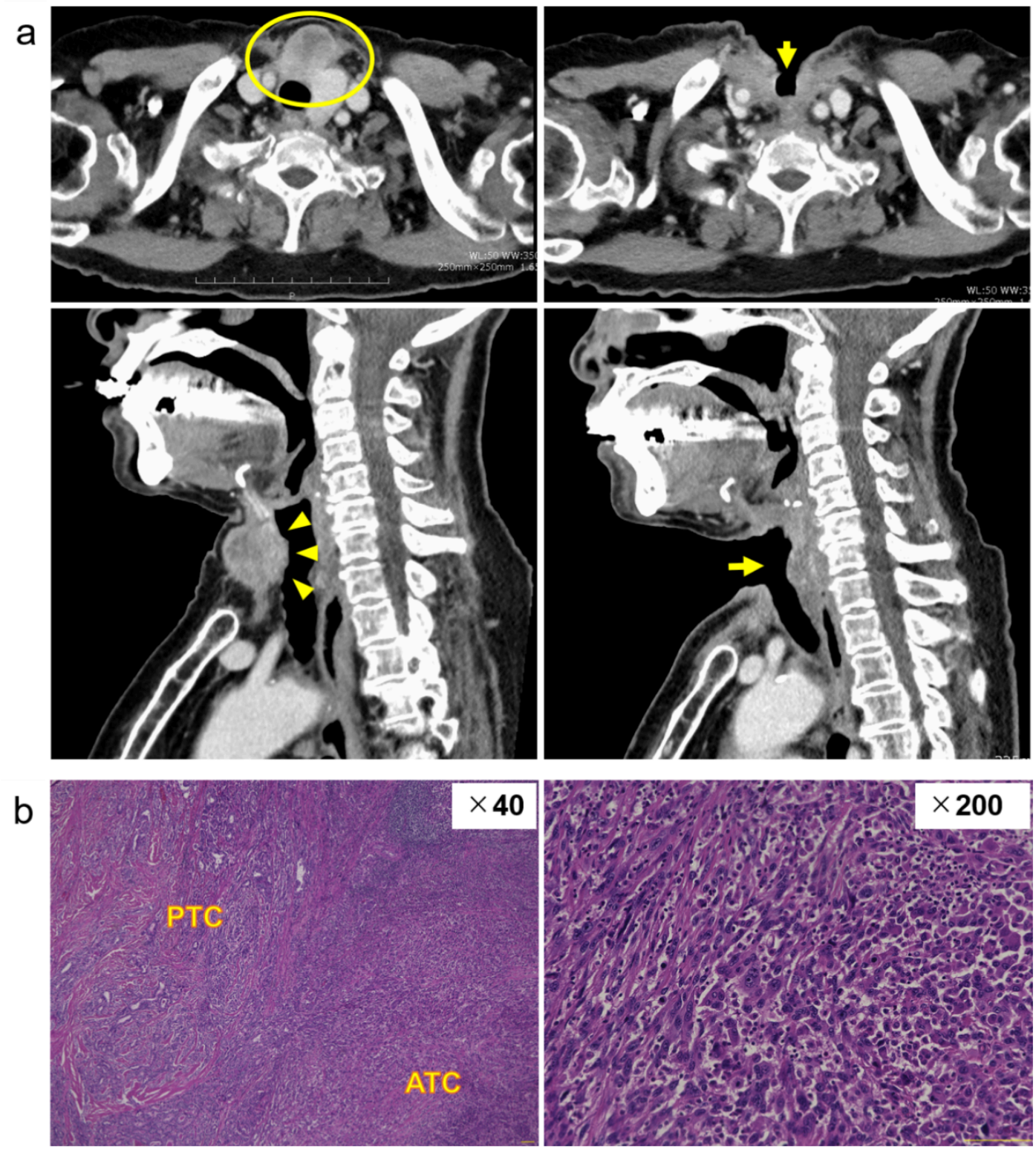


Figure 1

Clinical imaging and pathological features of the patient.

(a) Preoperative (left) and postoperative (right) contrast-enhanced CT scans (upper panels: axial view; lower panels: coronal view). The tumor is located in the thyroid isthmus (indicated by circles) with invasion into the anterior tracheal wall (indicated by arrowheads). The anterior tracheal wall was en bloc

resected from the cricoid cartilage to the third tracheal cartilage, creating a tracheostoma (indicated by arrows). **(b)** Hematoxylin and eosin (H&E) staining of the resected specimen. The findings demonstrate a transition from papillary thyroid carcinoma (PTC) to anaplastic thyroid carcinoma (ATC), leading to a diagnosis of ATC arising from PTC. Left: Low-magnification view (×40) capturing the PTC component (left side). Right: High-magnification view (×200) focusing on the ATC component. Scale bars represent 100 μm in both panels

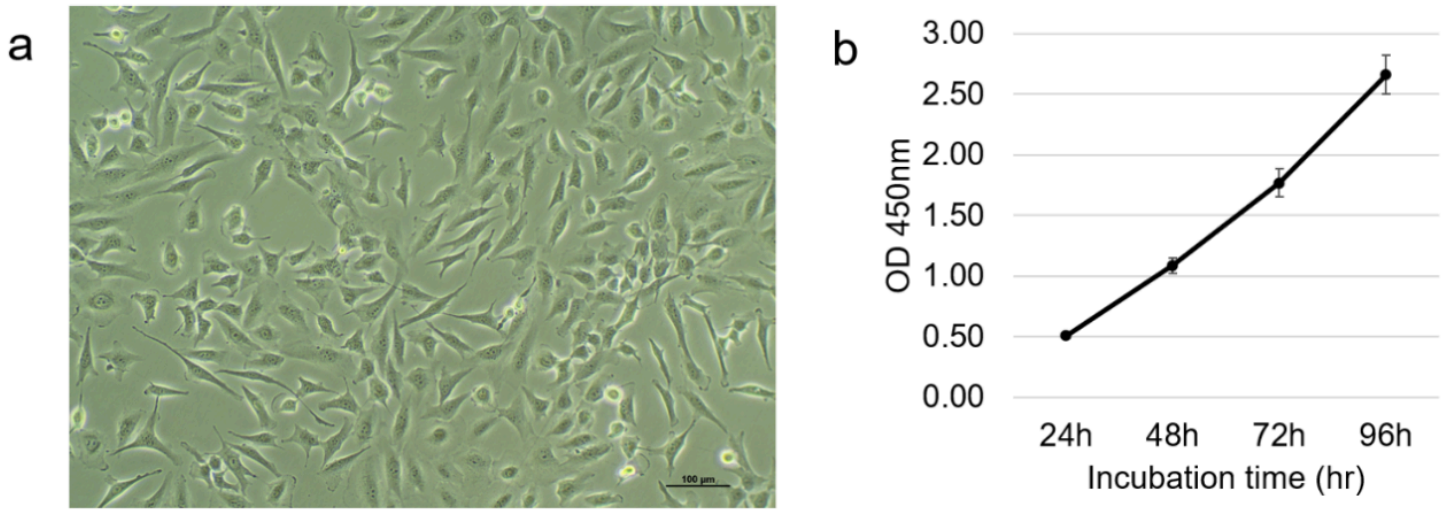


Figure 2

Cellular morphology and growth curve of OK-ATC1 cells.

(a) OK-ATC1 cells showed spindle-shaped and polygonal morphologies with prominent cytoplasmic extensions in DMEM (High Glucose) supplemented with 10% fetal bovine serum (FBS) and 1% penicillin-streptomycin (bar: 100 μm). **(b)** OK-ATC1 cells grew well in the medium with a doubling time of approximately 30 hours

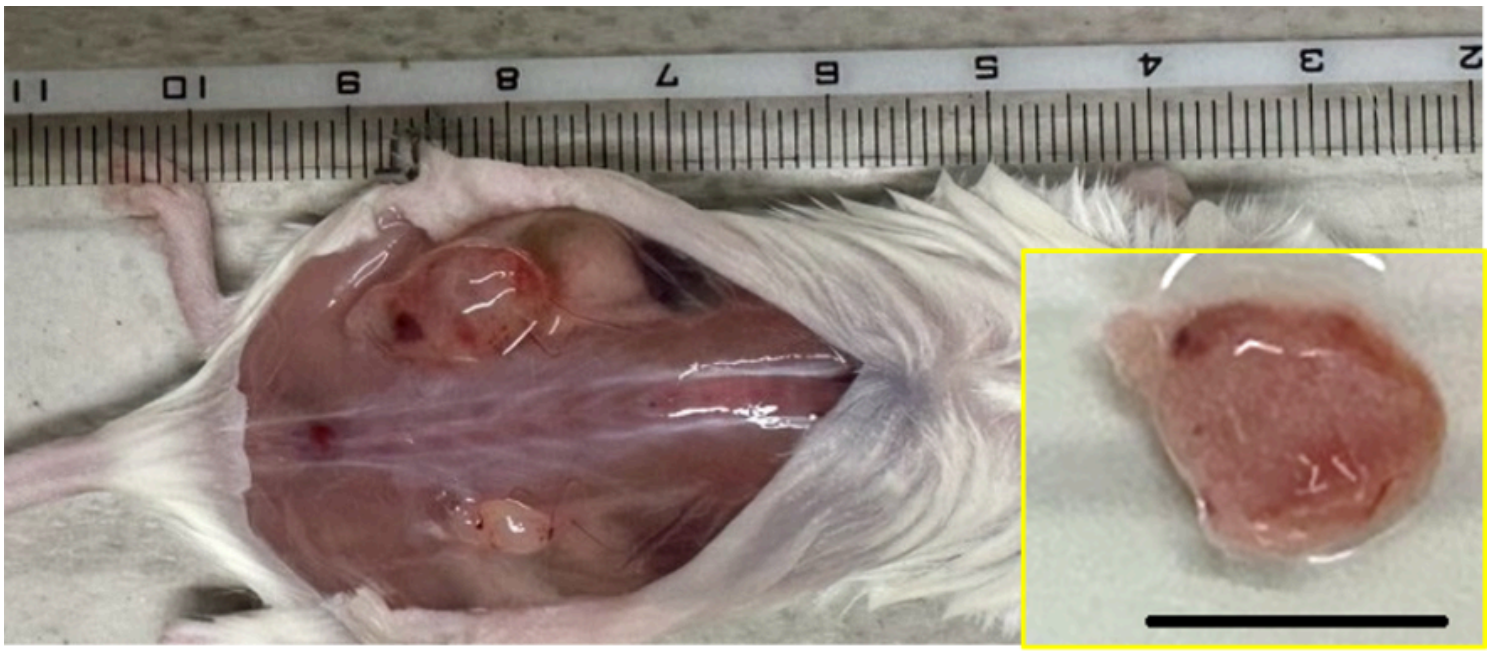


Figure 3

OK-ATC1-PDX tumors successfully engrafted in BRJ mice.

Representative photographs showing the actual tumors (passage 4) established by directly transplanting 5-mm tumor fragments into the bilateral flanks of Balb/c Rag2$^{-/-}$JAK3$^{-/-}$ (BRJ) mouse. The scale bar represents 1 cm. The harvested tumors were collected for subsequent histological evaluation, serial transplantation into the next generation, and cryopreservation

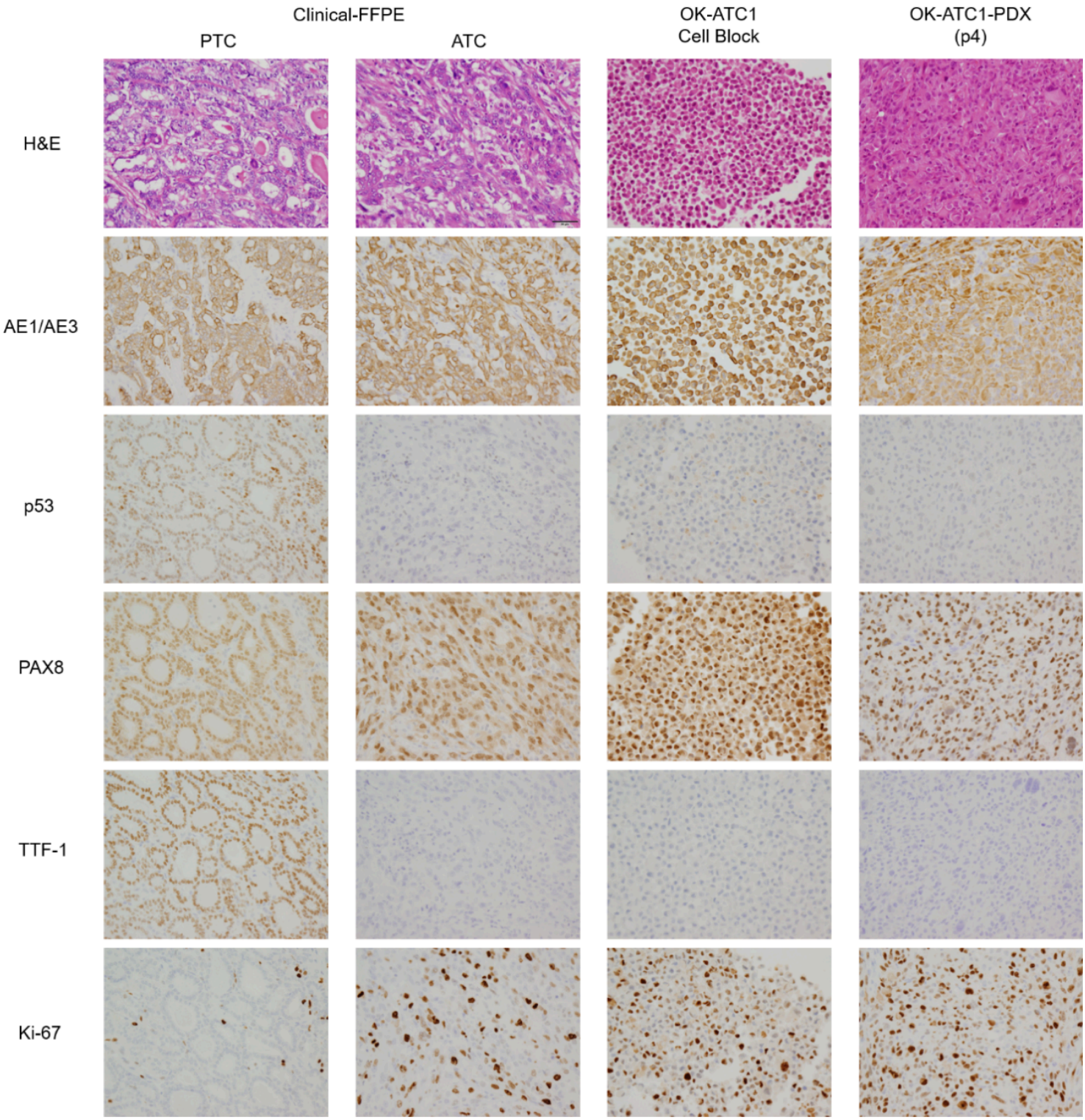


Figure 4

H&E and immunohistochemical staining of clinical samples (PTC and ATC components), OK-ATC1 cell blocks, and OK-ATC1-PDX at passage 4 (p4). Distinct staining patterns were observed between the papillary thyroid carcinoma (PTC) and anaplastic thyroid carcinoma (ATC) components, whereas the cell blocks and PDX exhibited staining profiles similar to those of the clinical ATC component. Detailed interpretations of these findings are summarized in Table 1. All images are shown at ×200 magnification. Scale bars represent 50 μm

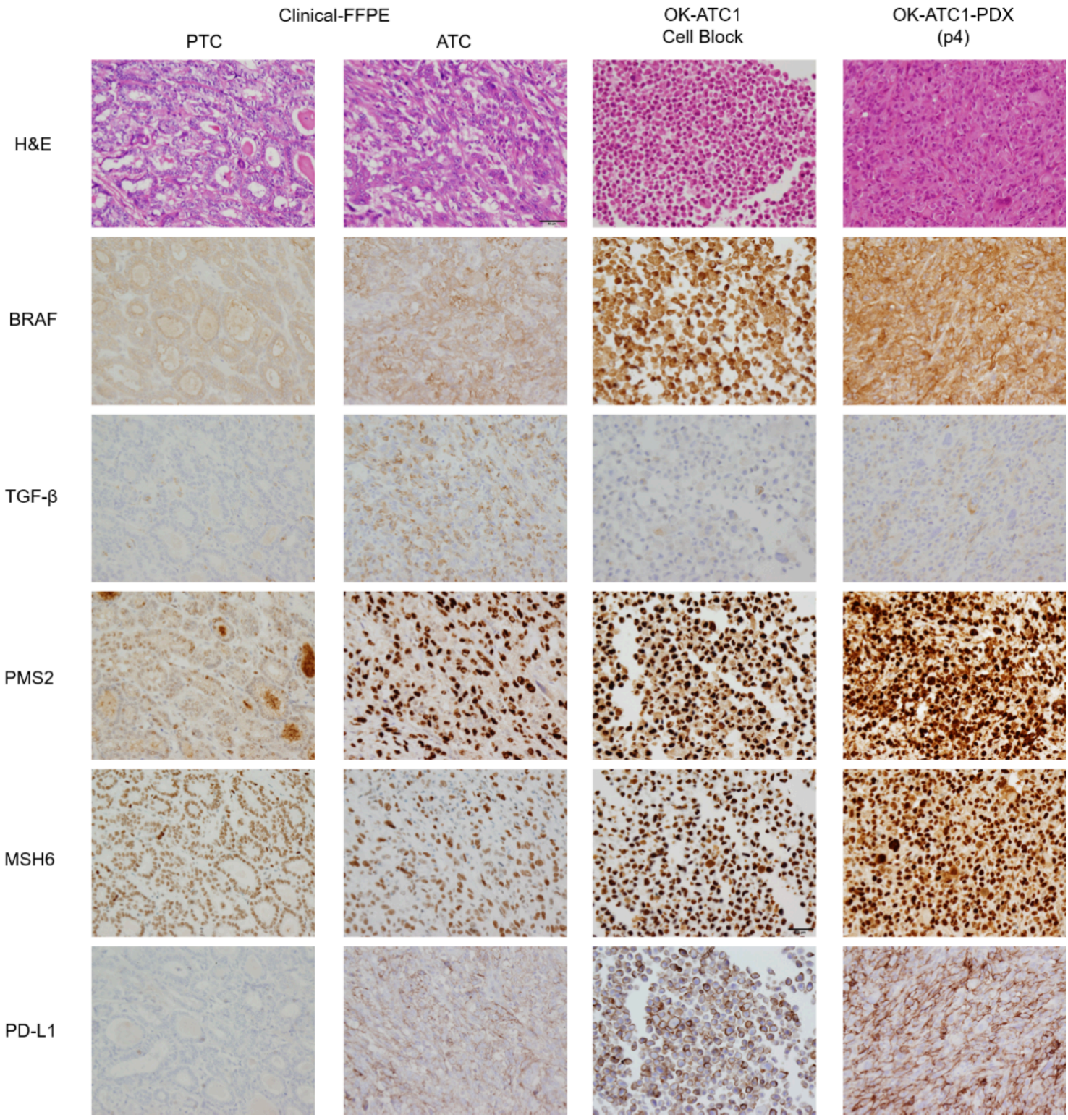
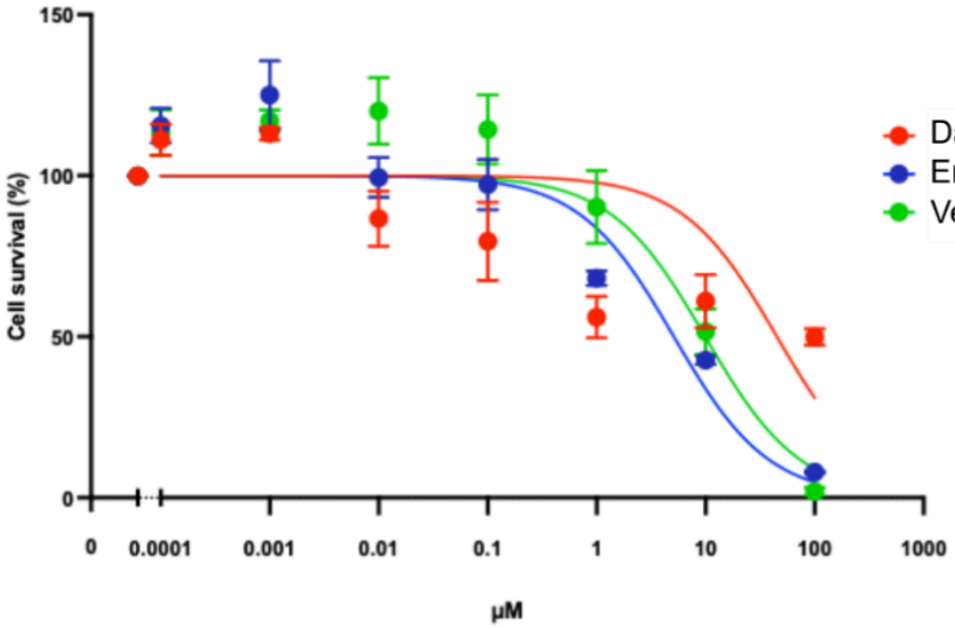


Figure 5

Immunohistochemical analysis of therapeutic targets and microenvironmental markers across clinical and established models.

All specimens showed positive staining for BRAF. TGF-β and PD-L1 were mostly absent in the PTC component but upregulated in ATC, with TGF-β exhibiting minimal expression in cell blocks. PMS2 also

showed weak staining in PTC but strong nuclear expression in ATC. MSH6 nuclear positivity was observed across all samples. Detailed interpretations of these findings are also summarized in Table 1. All images are shown at ×200 magnification



BRAF inhibitor	IC50 (μM)
Dabrafenib	45.1
Encorafenib	5.1
Vemurafenib	9.9

Figure 6

Sensitivity of OK-ATC1 cells to BRAF inhibitors.

The IC_{50} values for all three agents—dabrafenib, encorafenib, and vemurafenib—were at the micromolar level, suggesting intrinsic therapeutic resistance

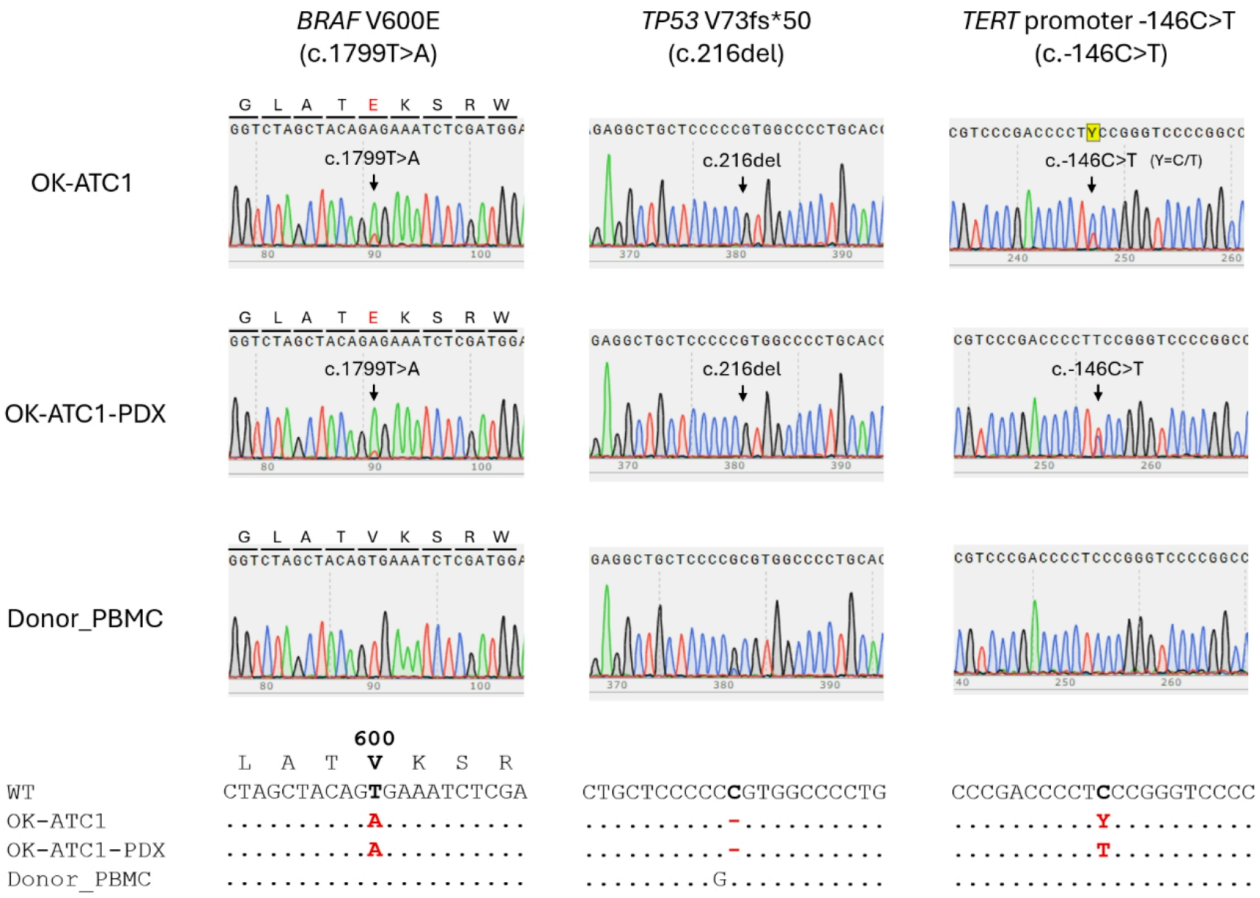


Figure 7

Validation of key driver mutations by Sanger sequencing.

Representative Sanger sequencing chromatograms of OK-ATC1 cells, the OK-ATC1-PDX model, and patient peripheral blood mononuclear cells (PBMCs). Nucleotide sequences indicating specific mutation sites for each gene are aligned below each chromatogram. Both OK-ATC1 cells and the OK-ATC1-PDX model harbored heterozygous *BRAF* V600E (c.1799T>A) and *TERT* promoter -146C>T (c.-146C>T) mutations, as well as a *TP53* V73fs*50 (c.216del) mutation. In contrast, patient PBMCs showed wild-type sequences for all corresponding driver mutations, although a heterozygous C/G single-nucleotide variant was observed at nucleotide position 215 of *TP53*. Reference sequences were obtained from the NCBI database for *BRAF*(NM_004333.4) and *TP53* (NM_000546.4), while the *TERT* promoter sequence was referenced from Panebianco et al. [16]

Supplementary Files

This is a list of supplementary files associated with this preprint. Click to download.

- supplementalTableFigure.docx